Original Article

Image quality, diagnostic performance of reduced-dose abdominal CT with artificial intelligence model-based iterative reconstruction for colorectal liver metastasis: a prospective cohort study

Qian-Sai Qiu[1,2#], Xiao-Shan Chen[1#], Wen-Tao Wang[1], Jia-Hui Wang[1], Cheng Yan[1], Min Ji[3], San-Yuan Dong[1], Meng-Su Zeng[1], Sheng-Xiang Rao[1]

[1]Department of Radiology, Zhongshan Hospital, Fudan University, Shanghai Institute of Medical Imaging, Shanghai, China; [2]Department of Radiology, Affiliated Tumor Hospital of Nantong University, Nantong University, Nantong, China; [3]Shanghai United Imaging Healthcare Co., Ltd., Shanghai, China

Contributions: (I) Conception and design: SX Rao; (II) Administrative support: SX Rao, MS Zeng; (III) Provision of study materials or patients: C Yan; (IV) Collection and assembly of data: QS Qiu, XS Chen; (V) Data analysis and interpretation: QS Qiu, M Ji; (VI) Manuscript writing: All authors; (VII) Final approval of manuscript: All authors.

[#]These authors contributed equally to this work.

Correspondence to: Sheng-Xiang Rao, PhD. Department of Radiology, Zhongshan Hospital, Fudan University, Shanghai Institute of Medical Imaging, No. 180 Fenglin Road, Xuhui District, Shanghai 200032, China. Email: raoxray@163.com.

Background: The optimization of regularization strategies in computed tomography (CT) iterative reconstruction may allow for a reduced dose (RD) without compromising image quality, thus the diagnostic ability of RD imaging must be considered, especially for low-contrast lesions. In this study, we evaluated the image quality and diagnostic performance of 50% RD CT for low-contrast colorectal liver metastasis (CRLM) with artificial intelligence model-based iterative reconstruction (AIIR) and standard-dose (SD) CT with hybrid iterative reconstruction (HIR).

Methods: In this prospective study, consecutive participants with pathologically proven colorectal cancer and suspected liver metastases who underwent portal venous phase CT scans both at SD and RD between June and November 2022 were included. All images were reconstructed by HIR and AIIR. Two radiologists detected and characterized liver lesions with RD HIR, SD HIR, and RD AIIR and scored the image quality. The contrast-to-noise ratio (CNR) for metastases were recorded. The diagnostic performance for CRLM of each reconstruction algorithm was analyzed and compared using the receiver operating characteristic curve and the area under the curves (AUC).

Results: A total of 56 participants with 422 liver lesions were recruited. The mean volume CT dose indices of the SD and RD scans were 9.5 and 4.8 mGy. RD AIIR exhibited superior subjective image quality and higher CNR for liver metastases than did RD/SD HIR. In all liver lesions and lesions ≤10 mm, the detection rates of RD AIIR (83.3% and 71.5%) were both significantly higher than those of RD HIR (76.3% and 62.4%; P=0.002 and P=0.003); meanwhile, they were similar to those of SD HIR (81.4% and 69.6%; P=0.307 and P=0.515). The AUCs of RD AIIR for all liver lesions and lesions ≤10 mm (0.858 and 0.764) were greater than those of RD HIR (0.781 and 0.661; P<0.001) and were similar to those of SD HIR (0.863 and 0.762; P=0.616 and 0.845).

Conclusions: AIIR can improve CT image quality at 50% RD while preserving diagnostic performance and confidence for low-contrast CRLM in all lesions and lesions ≤10 mm and may thus serve as a promising tool for follow-up monitoring in patients with colorectal cancer while inflicting less radiation damage.

Keywords: Artificial intelligence; model-based iterative reconstruction (MBIR); abdominal computed tomography (abdominal CT); reduced dose (RD); colorectal liver metastasis (CRLM)

Submitted Aug 01, 2024. Accepted for publication Jan 17, 2025. Published online Feb 18, 2025.
doi: 10.21037/qims-24-1570
View this article at: https://dx.doi.org/10.21037/qims-24-1570

Introduction

The distant metastasis of colorectal cancer commonly occurs in liver (1). The timely detection of colorectal liver metastasis (CRLM) is crucial for clinical management and the improvement of patient outcomes with appropriate treatment (2). The application of chest-abdomen-pelvic contrast-enhanced computed tomography (CT), the preferred screening protocol for patients with colorectal cancer (3,4), remains controversial due to its high radiation exposure. In recent years, promising deep learning-based image reconstruction (DLIR) algorithms have been developed that may reduce the required dose (5,6).

A recent study demonstrated that DLIR can improve perceptual CT imaging quality, signal-to-noise ratio (SNR), and contrast-to-noise ratio (CNR) in comparison to hybrid iterative reconstruction (HIR) and filtered back projection while maintaining the detectability of liver metastases larger than 0.5 cm at a 65% dose reduction (7). However, the study indicates that the DLIR should still be used with caution because of the overall inferior characterization of liver lesions and reader confidence. This could be caused by the complexity of deep learning networks, whose performance is highly dependent on the quality of training data. Other research suggests that DLIR could introduce hallucinated image features or miss image structures, particularly in low-dose settings (8,9).

Another method, conventional denoising framework model-based iterative reconstruction (MBIR), may have potential in facilitating reduced-dose (RD) CT scanning (10,11). In principle, MBIR takes the advantage of a statistical physical system model and a regularization term that can reduce noise and retain fine structural information in the image simultaneously. However, the regularization term in MBIR is often difficult to design. The most frequently used norm-based regularization terms can encourage unnatural piece-wise-constant "plastic texture" and may eliminate low contrast lesions in low-dose scans (6). In previous studies, how to maintain detectability of low-contrast lesions in MBIR images at low-dose scan remains to be demonstrated (12-14). In addition, due to its long reconstruction times, MBIR is not commonly adopted for clinical application.

Recently, a hybrid reconstruction algorithm that integrates deep learning-based reconstruction and MBIR was proposed to reconstruct high-quality images from low-dose CT scans. Subsequently, the artificial intelligence model-based iterative reconstruction (AIIR; United Imaging Healthcare, Shanghai, China) algorithm was developed with the advantages of denoising capability and raw data fidelity. In initial validation, this algorithm achieved promising performance in reconstructing ultra-low-dose CT images with high spatial resolution, reduced noise and artifacts, and improved low-contrast detectability (15). Several previous clinical studies of AIIR have indicated its superior image quality in CT angiography and thoracic imaging (16,17). We hypothesize that AIIR can also improve image quality and maintain detection and characterization for small low-contrast lesions. We aimed to evaluate the objective image quality and the detectability of low-contrast CRLM provided by RD AIIR and standard-dose (SD)/RD HIR for portal venous phase abdominal CT scans through an observation study (16-18). We present this article in accordance with the STROBE reporting checklist (available at https://qims.amegroups.com/article/view/10.21037/qims-24-1570/rc).

Methods

The study was conducted in accordance with the Declaration of Helsinki (as revised in 2013) and was approved by the Ethics Committee of Zhongshan Hospital, Fudan University (No. B2022-127R). Informed consent was obtained from all individual participants.

Participant population

This single-center prospective cohort study was conducted in Zhongshan Hospital, Fudan University, from June to November 2022, with 159 consecutive patients undergoing

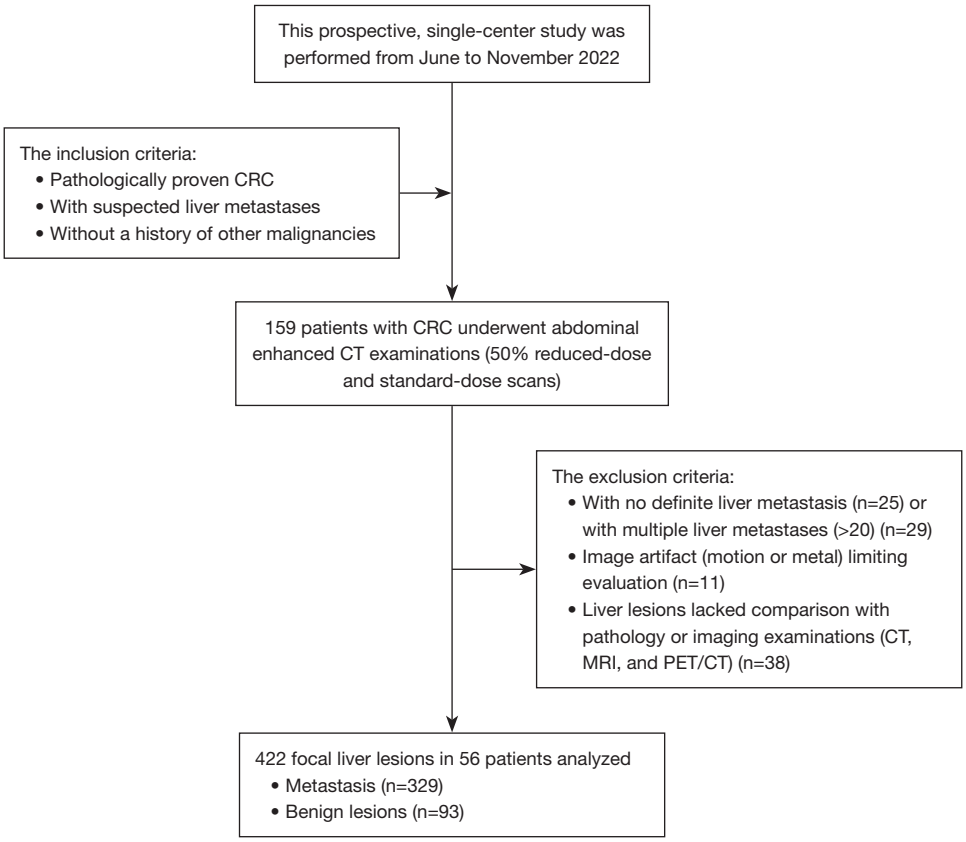

Figure 1 Flowchart of the study. CRC, colorectal cancer; CT, computed tomography; MRI, magnetic resonance imaging; PET, positron emission tomography.

abdominal enhanced CT examinations (50% RD and SD scans). The inclusion and exclusion criteria are listed in *Figure 1*. Each participant's age, sex, height, weight, and body mass index were recorded. Follow-up of the participants occurred through May 2023.

Imaging technique and postprocessing

All CT scans were obtained using a multislice CT scanner (uCT960+, United Imaging Healthcare). All participants underwent CT of the abdomen in the portal venous phase, and the details of scan parameters are provided in *Table 1*. The RD parameters were set to approximately 50% the standard radiation dose. SD and RD scans were performed in the craniocaudal direction and then in the opposite direction during the same breath-hold with minimal delay time.

Weight-based intravenous injection of contrast material was used with iomeprol and 300 mg of iodine per milliliter (Shanghai Borui KeXinYi Pharmaceutical Co., Shanghai, China) under a setting of 1.3 mL/kg and an injection rate of 3 mL/s. Bolus tracking was used, with a 200-Hounsfield unit (HU) trigger value in the abdominal aorta at the level of the celiac artery and a scan delay of 10 s for the arterial-phase scan and another 40 s for the portal-phase scan. Three reconstructions at a 1-mm slice thickness were performed for each participant: one at standard radiation doses (HIR) and two at reduced radiation doses (HIR and AIIR). The details of AIIR algorithm are provided in Appendix 1.

Qualitative analysis of image quality

For each patient, images from three protocols (RD HIR, SD HIR, and RD AIIR) were independently assessed by two radiologists (readers 1 and 2, one junior and one senior with 5 and 16 years of experience in the field of abdominal imaging diagnosis, respectively). The window width and window level of the images could be freely adjusted on a MDNG3421 monitor (Barco, Kortrijk, Belgium). The

Table 1 Scan parameters for the abdominal CT protocol

Parameter	Datum
Scan model	Helical, single source
Pitch factor	0.9937
Rotation time (s)	0.5
Tube current modulation (noise index/minimum mA)	
SD scan	Scan-by-scan settings for approximating the prior standard scan (index level 2 or reference mAs—160 mAs)
RD scan	Scan-by-scan settings for approximating a 50% dose reduction
Tube potential (kV)	120
Collimation width (mm)	40
Reconstruction thickness and increment (mm)	1/1
Matrix size (no. of pixels)	512×512
Reconstruction algorithm	
HIR	B_SOFT_B Kernel, KARL 3D level 3
AIIR	Strength level 3 (maximum level is 5)

RD, reduced dose; SD, standard dose; HIR, hybrid iterative technique; AIIR, artificial intelligence model-based iterative reconstruction; CT, computed tomography.

overall image quality was scored based on the assessment of imaging noise, intrahepatic vascularity, liver focal lesions, and other abdominal organs. The scoring scheme was as follows: 5, excellent image quality without related issues of concern, 4, minor issues not interfering with diagnostic decision making; 3, minor issues possibly interfering with diagnostic decision making; 2, major issues affecting visualization of major structures but diagnosis still possible; and 1, issues affecting diagnostic information.

Quantitative analysis of image quality

The image noise and CT number were measured by reader 1, using United Imaging Advantage Workstation software (R004; United Imaging Healthcare). Circular regions of interest (ROIs) were drawn in the liver (one for each of the left lateral lobe, left medial lobe, right anterior lobe, and right posterior lobe), psoas muscle (one left and one right), subcutaneous fat (one anterior and one posterior), and within the single largest liver metastasis per participant, with confounding structures such as large vessels being avoided. The image noise and CT number for liver, fat, and muscle were defined as their mean values in corresponding ROI measurements. SNR and CNR were calculated using the following equations, respectively: SNR = mean CT number/SD; CNR_{liver} = mean CT $number_{(liver - muscle)}/SD_{fat}$; $CNR_{metastasis}$ = mean CT $number_{(liver - metastasis)}/SD_{fat}$.

Liver lesion detection and characterization

Three image sets of different doses and reconstructions were reviewed by readers 1 and 2 respectively, and a 4-week interval was set between the interpretations to minimize the bias. The readers knew that colorectal cancer was present in patients, but they did not know whether liver lesions were present or the pathological results. Each liver lesion was recorded with the presence, location, and size and then classified via a 5-point scale (with 1 indicating definitely benign and 5 indicating definitely malignant). If the lesion received a score of ≥3, it was considered CRLM; otherwise, it was considered benign. A radiologist (reader 3) not involved in imaging interpretation annotated all lesions with access to prior and future available cross-sectional imaging examinations [CT, magnetic resonance imaging (MRI), and positron emission tomography-CT], as well as clinical data. All patients were followed up for at least 6 months. Previously equivocal lesions could be distinguished as metastases or benign lesions based on whether obvious

Table 2 Participant and lesion characteristics

Parameter	Value (N=56)
Age (years)	60.5±12.4
Sex	
Male	45 (80.4)
Female	11 (19.6)
Location of primary cancer	
Colon	37 (66.1)
Rectum	19 (33.9)
Prior chemotherapy	
Yes	36 (64.3)
No	20 (35.7)
Fatty liver	
Yes	6 (10.7)
No	50 (89.3)
Body mass index (kg/m^2)	23.0±3.2
Liver lesions	
No. of liver lesions	422
No. of malignant lesions	329 (78.0)
No. of benign lesions	93 (22.0)
Lesion size (mm)	13.6±13.7

Data are presented as mean ± standard deviation, number or number (percentage).

lesion size enlargement occurred. For participants with 20 or more metastatic lesions, lesion performance was not assessed. CRLMs manifest on portal venous phase CT as hypovascular nodules with irregular peripheral enhancement. The criteria for liver metastasis on MRI were as follows: (I) mild-to-moderate high signal intensity on T2-weighted imaging (T2WI); (II) diffusion restriction, with a higher signal on diffusion-weighted imaging (DWI) and a lower or similar signal to that of the liver on apparent diffusion coefficient (ADC); and (III) irregular peripheral enhancement during the arterial phase or portal venous phase.

Statistical analysis

Statistical analysis was conducted using SPSS version 24.0 (IBM Corp., Armonk, NY, USA). Continuous variables conforming to a normal distribution are represented as mean ± standard deviation and were compared with the paired-samples *t*-test; otherwise, they are presented as the median and interquartile range and were compared via the Wilcoxon signed-rank test. Classification variables are expressed as frequency (percentages) and were compared with the McNemar chi-squared test. The per-lesion sensitivity, specificity, positive predictive value, negative predictive value, and accuracy of three protocols were calculated. The diagnostic performance for liver metastases was assessed by conducting receiver operating characteristic (ROC) analysis, and the areas under the curve (AUCs) were calculated and pairwise compared using a univariate z score test. Tukey-Kramer adjustment was used to control the overall type I error rate at 5%. A subgroup analysis was conducted based on the lesions size (≤10 and >10 mm). Interobserver agreement for the disease detection and the classification of each protocol were evaluated with Cohen kappa statistics. κ values of 0.01–0.20 were considered slight; 0.21–0.40, fair; 0.41–0.60, moderate; 0.61–0.80, substantial; and 0.81–1.0, excellent. A two-sided P value <0.05 was considered statistically significant.

Results

Patient demographics and lesion characteristics

The patient demographics are summarized in *Table 2*. The final patient cohort consisted of 56 participants (45 males and 11 females) with a mean age of 60.5±12.4 years (range, 33–85 years) and a mean body mass index of 23.0±3.2 kg/m^2 (range, 16.8–32.1 kg/m^2).

A total of 422 focal liver lesions were evaluated in the study (329 metastatic and 93 benign lesions including 79 cysts and 14 hemangiomas), with a mean size of 13.6±13.7 mm (range, 1–162 mm). Metastases were confirmed by pathology after surgical resection of the lesions (n=43) or confirmed based on available cross-sectional imaging examinations and clinical data (n=286). Details of the lesion characteristics are provided in *Table 2*.

Radiation dose

For SD scans, the mean volume CT dose index ($CTDI_{vol}$) was 9.5±1.8 mGy (range, 7.2–14.7 mGy). For RD scans, the mean $CTDI_{vol}$ was 4.8±0.9 mGy (range, 3.5–6.9 mGy).

Qualitative image assessment

Figure 2 shows the superiority of RD AIIR over RD HIR

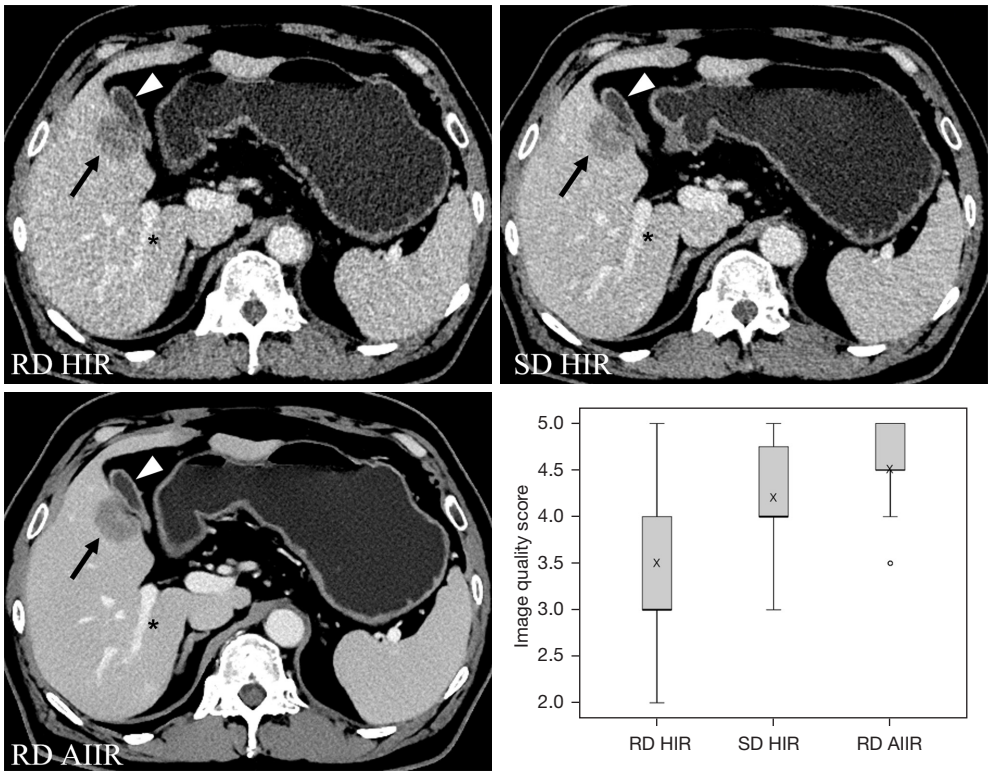

Figure 2 Axial contrast-enhanced CT images of the abdomen in a 59-year-old man obtained with SD (8.73 mGy) and RD (4.45 mGy). Based on the visual noise of the liver, the display of the blood vessel (i.e., right posterior branch of portal vein, black stars) and surrounding organs (i.e., gallbladder, white arrows), the subjective scores of image quality were 3, 4, and 5 for RD HIR, SD HIR, and RD AIIR, respectively. The box-and-whisker plot shows the results of the qualitative evaluation of the overall image quality score. The X is the data mean. The mean image quality score was significantly different between each reconstruction based on the pairwise comparison (P<0.001). A 33-mm low-contrast left liver metastasis (black arrows) was scored as 5 by both readers with each reconstruction, and the contrast-to-noise ratios for liver metastases in this participant for RD HIR, SD HIR, and RD AIIR were 2.7, 3.4, and 4.7, respectively. RD, reduced dose; SD, standard dose; HIR, hybrid iterative reconstruction; AIIR, artificial intelligence model-based iterative reconstruction; CT, computed tomography.

and SD HIR in terms of image noise and the visualization of intrahepatic vessels, liver lesions, and other abdominal organs. The mean image quality scores for RD HIR, SD HIR. and RD AIIR were 3.5±0.7, 4.2±0.6, and 4.5±0.4, respectively, and the differences between the pairings were statistically significant (P<0.001).

Quantitative image assessment

The CT number and noise measurements with the SNR and CNR calculations are shown in *Table 3*. There was no statistical difference in CT number (liver, metastases, and psoas muscle) between the different dose and reconstructions. Nevertheless, RD AIIR had a significantly higher SNR and CNR than did RD HIR and SD HIR.

Detection rates

RD HIR detected 322 of the 422 lesions (76.3%) and 234 of the 329 (71.1%) metastases, SD HIR detected 343.5 of the 422 lesions (81.4%) and 255 of the 329 metastases (77.5%), and RD AIIR detected 351.5 of the 422 lesions (83.3%) and 260.5 of the 329 (79.2%) metastases. The detection rates between RD HIR and SD HIR were significantly different for all lesions (P=0.010), for lesions ≤10 mm (P=0.022), and for metastases (P=0.008); however, there was no statistical difference for lesions >10 mm (P=0.120). The detection rates were significantly different between RD HIR and

Table 3 CT number, noise, SNR, and CNR in the abdomen according to dose and reconstruction method

Variable	RD HIR	SD HIR	RD AIIR
CT number (HU)[#]	100.4 (92.4, 106.2)	100.2 (92.1, 106.7)	100.4 (94.2, 106.9)
Liver			
Metastases[†]	56.9±18.0	56.4±19.8	55.6±19.2
Psoas muscle	55.4±7.2	55.2±6.3	54.6±6.0
Noise[‡]			
Liver	13.7±1.5	12.0±1.9	6.7±1.0
Subcutaneous fat	12.6±1.9	10.6±1.6	6.7±1.5
SNR[§]			
Liver	7.2±1.4	8.3±1.7	15.0±3.5
Metastases	3.9±1.4	4.9±2.5	7.3±3.0
CNR[§]			
Liver	3.5±1.2	4.1±1.3	6.9±2.3
Metastases	3.4±1.5	4.0±1.7	6.9±3.0

Data are presented as median (interquartile range) or mean ± standard deviation. [#], no significant difference in CT number was identified between different dose and reconstructions. [†], the CT number of the single largest representative lesion fulfilling the study criteria was measured in each applicable participant. [‡], noise = CT number standard deviation in the liver and subcutaneous fat. Noise was significantly different across all the groups (P<0.05). [§], SNR and CNR were significantly different across different doses and reconstructions (P<0.05). The techniques ranked from highest to lowest according to SNR and CNR were as follows: RD AIIR, SD HIR, and RD HIR. RD, reduced dose; SD, standard dose; HIR, hybrid iterative reconstruction; AIIR, artificial intelligence model-based iterative reconstruction; CNR, contrast-to-noise ratio; SNR, signal-to-noise ratio; CT, computed tomography.

RD AIIR for all lesions, lesions ≤10 mm, lesions >10 mm, and metastases (P=0.001–0.004). However, the detection rates were insignificantly different between SD HIR and RD AIIR for all groups (P=0.170–0.515). Details regarding the detection rates are shown in *Table 4* and Table S1. This inferior detection ability was mainly due to the increase of image noise caused by radiation dose reduction and the small size and hidden location (e.g., under the liver capsule) of low-contrast lesions (*Figures 3*,*4*). Figure S1 shows metastasis in hepatic segment 1 that could be interpreted as extrahepatic lesion compression.

Per lesion-based diagnostic performance

The diagnostic performance for liver metastases with different doses and reconstruction methods by readers 1 and 2 is shown in Table S2. Overall, the AUCs of RD HIR were 0.787 [95% confidence interval (CI): 0.751–0.822], the AUCs of SD HIR were 0.863 (95% CI: 0.836–0.886), and the AUCs of RD AIIR were 0.858 (95% CI: 0.831–0.886).

In all lesions and lesions ≤10 mm, the AUCs of RD HIR were inferior to those of SD HIR and RD AIIR (P<0.001), while the AUCs of RD AIIR were similar to those of SD HIR (P=0.616 and P=0.845, respectively). Details on the comparison of AUCs are shown in *Table 5*. Figure S2 shows a 2-mm liver cyst with false-positive characterizations both at RD and SD scans, with RD AIIR resulting in true-negative characterizations by two readers.

Diagnostic confidence

RD AIIR, as compared with RD HIR and SD HIR, had a significantly higher percentage of score 4 and above (17.3% and 41.9%, respectively) among 329 metastases and a lower percentage of missed diagnoses (20.8%) (*Figure 5*). Table S3 presents the scoring details of all lesions by readers 1 and 2. RD AIIR had higher scores for low-contrast liver metastases than did both HIR modes (Figures S3,S4).

Interobserver agreement

The interobserver agreement in disease detection and

Table 4 Detection rates in all lesions and metastases

Group	RD HIR (I)	SD HIR (II)	RD AIIR (III)	P value		
				I *vs.* II	I *vs.* III	II *vs.* III
All lesions (%)	76.3 (72.2–80.4) [322/422]	81.4 (77.6–85.1) [343.5/422]	83.3 (79.6–86.8) [351.5/422]	0.010	0.002	0.307
≤10 mm (%)	62.4 (56.0–68.6) [143.5/230]	69.6 (63.6–75.6) [160/230]	71.5 (65.6–77.3) [164.5/230]	0.022	0.003	0.515
>10 mm (%)	93.0 (89.1–96.4) [178.5/192]	95.6 (92.3–98.3) [183.5/192]	97.4 (95.1–99.7) [187/192]	0.120	0.004	0.170
Metastases (%)	71.1 (66.2–76.0) [234/329]	77.5 (73.0–82.0) [255/329]	79.2 (74.7–83.5) [260.5/329]	0.008	0.001	0.462

Performance data are per lesion. Numbers in parentheses are the 95% CIs, and the numbers in brackets are the numbers of lesions. RD, reduced dose; SD, standard dose; HIR, hybrid iterative reconstruction; AIIR, artificial intelligence model-based iterative reconstruction; CI, confidence interval.

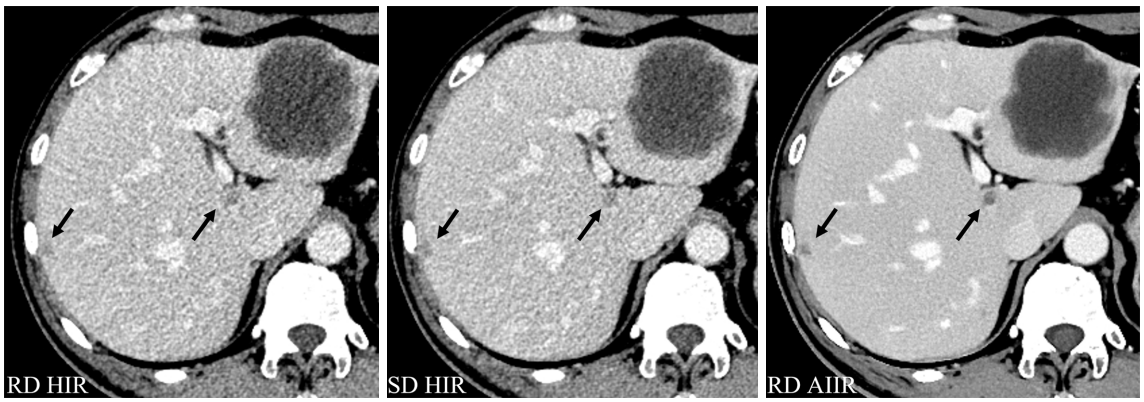

Figure 3 Axial contrast-enhanced CT images of the abdomen in a 51-year-old man with three liver metastases. A 65-mm lesion in hepatic segment 3 had obvious necrosis that was considered to be a large cyst by reader 1 under RD HIR. However, under SD HIR and particularly under RD AIIR, the solid components of the lesion edge could be clearly displayed. Due to the hidden location of lesions, the other two lesions (under the liver capsule of segment 5 and segment 1, black arrows) were missed by both readers with RD HIR but were detected with SD HIR and with RD AIIR. Of note, the two lesions were scored 4 with RD AIIR, which was superior to both the SD HIR scores (3 for both readers). CT, computed tomography; RD, reduced dose; SD, standard dose; HIR, hybrid iterative reconstruction; AIIR, artificial intelligence model-based iterative reconstruction.

classification for RD HIR, SD HIR, and RD AIIR were substantial, with the κ values above 0.80 (Table S4).

Discussion

As the preferred radiological modality for the evaluation of distant metastases of colorectal cancer, chest-abdomen-pelvic CT with intravenous contrast administration is questioned due to radiation exposure, while dose reduction limits the detection and classification of low-contrast liver lesions. Our study demonstrated that AIIR increased the perceptual imaging quality, SNR, and CNR of 50%-RD CT compared to both RD HIR and SD HIR. Moreover, RD AIIR showed a comparable diagnostic performance for CRLM with that of SD HIR and was significantly superior to RD HIR ($P<0.05$) in all lesions and lesions ≤10 mm, providing greater diagnostic confidence. This suggests that 50%-RD AIIR can replace SD HIR for follow-up surveillance of liver metastases in patients with colorectal cancer, who can benefit from its superior denoising capability.

Based on previous research, thick slices of 2–4 mm rather than 1 mm are recommended for axial imaging due to the associated increase in noise and damage to image quality, although thin slice thickness improves CRLM detection (19). In this study, the higher image noise was due to the thin reconstruction thickness of 1 mm of HIR at 100% radiation dose (mean hepatic parenchymal noise of

Figure 4 Axial contrast-enhanced CT images of the abdomen in a 49-year-old woman with two liver metastases in hepatic segment 6. A 14-mm low-contrast lesion (black arrows) was detected by both readers, and the CNRs for RD HIR, SD HIR, and RD AIIR were 1.5, 2.2, and 3.4, respectively. A 4-mm lesion (circles) was missed with RD HIR and SD HIR by both readers but was detected with RD AIIR; the scores from reader 1 and reader 2 were 3 and 4, respectively. RD, reduced dose; SD, standard dose; HIR, hybrid iterative reconstruction; AIIR, artificial intelligence model-based iterative reconstruction; CNR, contrast-to-noise ratio; CT, computed tomography.

Table 5 Comparison of AUCs of different doses and reconstructions in subgroup analysis

Group	RD HIR (I)	SD HIR (II)	RD AIIR (III)	I *vs.* II		I *vs.* III		II *vs.* III	
				z	P value	z	P value	z	P value
All lesions	0.787 (0.751–0.822)	0.863 (0.836–0.886)	0.858 (0.831–0.886)	6.504	<0.001	5.729	<0.001	0.502	0.616
≤10 mm	0.661 (0.608–0.713)	0.762 (0.717–0.806)	0.764 (0.720–0.808)	6.149	<0.001	5.646	<0.001	0.195	0.845
>10 mm	0.939 (0.905–0.973)	0.977 (0.964–0.991)	0.957 (0.925–0.989)	2.693	0.007	3.207	0.001	1.463	0.143

Performance data are per lesion. Numbers in parentheses are 95% CIs. RD, reduced dose; SD, standard dose; HIR, hybrid iterative reconstruction; AIIR, artificial intelligence model-based iterative reconstruction; AUC, area under the curve; CI, confidence interval.

12.0), which was further increased if the radiation dose was reduced by 50% (mean hepatic parenchymal noise of 13.7). However, AIIR combined with the artificial intelligence-based MBIR algorithm could significantly reduce image noise (mean hepatic parenchymal noise of 6.7) at 50% RD and demonstrated significantly superior image quality to that of RD and SD HIR. Moreover, the image spatial resolution was also preserved in AIIR. Our phantom test showed that the task transfer function was well maintained with a RD in AIIR for different contrast objects, implying a stronger correlation between image noise and actual image quality (Table S5).

As an advanced reconstruction algorithm for CT studies, MBIR, unlike HIR, works on both the acquisition process, including the system optics and quantum noise statistic, which can improve the image quality and allow for a radiation-dose reduction (10,11,20). Nonetheless, the improved detectability on MBIR images of low-contrast lesions, particularly at low-dose tube flux levels and in larger patients, remains to be demonstrated (12-14). The possible reason for this is that the performance of manually designed regularization functions will result in the unusual behavior

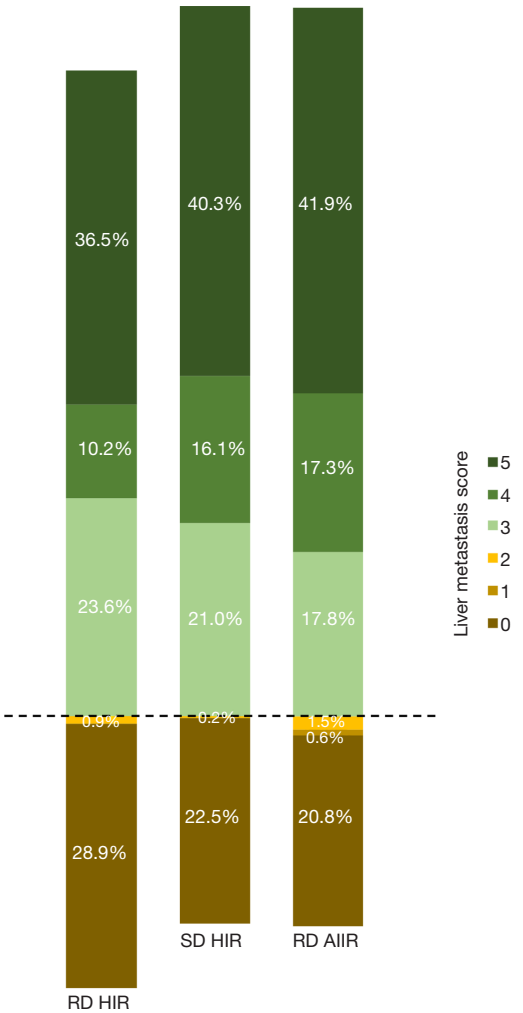

Figure 5 Score distributions of 329 cases of liver metastases for RD HIR, SD HIR, and RD AIIR. Lesions with a score of ≥3 were considered CRLMs; otherwise, they were considered benign lesions (dotted line represents the boundary). Overall, there were 77.5 (23.6%), 33.5 (10.2%), and 129 (36.5%) true-positive lesions that were scored from 3 to 5 respectively for RD HIR; 69 (21.0%), 53 (16.1%), and 132.5 (40.3%) for SD HIR; and 58.5 (17.8%), 57 (17.3%), and 138 (41.9%) for RD AIIR. The number of false-negatives lesions (scored of 1 and 2) generated by RD HIR, SD HIR, and RD AIIR was 3 (0.9%), 0.5 (0.2%), and 7 (2.1%), respectively; meanwhile, RD HIR, SD HIR, and RD AIIR missed 95 (28.9%), 74 (22.5%), and 68.5 (20.8%) of the lesions that were scored 0, respectively. RD, reduced dose; SD, standard dose; HIR, hybrid iterative reconstruction; AIIR, artificial intelligence model-based iterative reconstruction.

of modulation transfer function and unnatural image texture, such as plastic-looking appearances, which are usually more severe when the scan dose is lower in MBIR. In Richard *et al.*'s work, the task-based modulation transfer function for MBIR was greater than that for filtered back projection at a high dose and a contrast object of 900 HU; however, the performance diminished at a low dose and a contrast object of 120 HU. In contrast, modulation transfer function (MTF) for adaptive statistical iterative reconstruction (ASIR) remained equal or slightly lower as compared to filtered back projection in the set of imaging conditions (21,22). This could explain why MBIR at a low dose shows inferior performance in low contrast tasks, such as in CRLM, which has an even lower 50-HU contrast.

In this study, we replaced the manual regularization design with a deep learning-based regularization function. With the help of millions of parameters in the deep learning network, the deep learning-based regularization model is able to describe the image characteristics with more detailed features that cannot be predefined in the traditional MBIR regularization function. Hence, accompanied by remarkable noise reduction, AIIR showed significantly better diagnostic performance for CRLM than did HIR in the 50% low-dose scan and was comparable to HIR in the SD scan. In addition, the addition of deep learning could shorten reconstruction times with the help of fast-developing artificial intelligence hardware.

Many previous studies have applied deep learning techniques to image reconstruction to improve image quality and reduce the CT radiation dose (9,23-25) but only a limited number of studies have focused on low-contrast lesions such as CRLM. Jensen *et al.* reported that the DLIR, as compared to SD filtered back projection, improved CT image quality at a 65% radiation dose reduction while preserving the detection of liver lesions larger than 0.5 cm. However, for small lesions (<0.5 cm), the observer lesion characterization, confidence, and detection were inferior for low-contrast liver lesions with RD DLIR (7). Based on the inherent limitations of CT, our subgroup analysis included liver lesions ≤10 mm rather than smaller-size lesions, and we found that the detection and AUC values for the CRLM of AIIR-reconstructed CT images at a 50% radiation dose reduction were still not inferior to those of HIR CT images at a standard dose. This may be explained by the slice thickness being 1 mm

thinner than that reported in previous research. Another study indicated that DLIR was noninferior for small lesions (<1 cm) at dose reductions of no greater than 50% compared to full-dose filtered back projection or iterative reconstruction and that it maintained a noninferior image quality (26). However, there were decreasing scores on all image quality metrics and lesion assessments with decreasing dose levels. In our study, the 50% RD CT images reconstructed by AIIR had even better image quality than did SD CT images reconstructed by HIR. Furthermore, based on the analysis of lesions scores, unlike HIR, there was no impairment in diagnostic confidence for CRLM with RD CT images reconstructed via AIIR. In another study by Park *et al.* (27), the qualitative analysis indicated that MBIR applied to SD CT provided better image quality than did low-dose computed tomography (LDCT) combined with a deep learning denoising algorithm (P<0.05) but did not yield equal detectability for malignant or potentially malignant liver lesions as compared with SD CT. Moreover, the DLIR was directly applied on MBIR image as postprocessing, and the raw data were not fully incorporated into iterative process as is done in AIIR. Although previous studies have demonstrated that DLIR can maintain the high-contrast spatial resolution of RD CT images, progressively higher strengths of DLIR have been reported to result in minor blurring of tiny liver lesions and vessels (28). This can be likely attributed to the lack of information provided by the raw data such as in MBIR.

This study had several limitations that should be acknowledged. First, we employed a single-center design with a relatively small sample size, and we will expand the scope to further validate and our findings. Second, radiation exposure is a concern that is considered in the design of clinical research for patient safety. Therefore, we evaluated only the SD and the 50% RD with reference to previous studies. Furthermore, after we simplified the delayed-phase scans, additional low-dose scans did not increase the overall radiation exposure of patients. Third, the MBIR combined with the artificial intelligence algorithm was developed by a single vendor and only applied in one scanner model. Fourth, although each participant had biopsy-confirmed colorectal cancer, the characterization of most liver lesions in the reference standard was based on imaging diagnosis.

Conclusions

An artificial intelligence algorithm combined with MBIR could greatly improve both subjective and objective image quality as compared to that of HIR. In addition, our study revealed that the AIIR provided high diagnostic confidence and superior diagnostic performance for CRLM as compared with HIR at a 50% radiation dose reduction in all lesions and in lesions ≤10 mm while showing comparable performance to that of HIR at a standard radiation dose. Thus, AIIR could facilitate the application of a 50% RD CT scan for follow-up monitoring in colorectal cancer and thus reduce the radiation damage patients are subjected to without compromising the diagnostic efficacy for CRLM.

Acknowledgments

None.

Footnote

Reporting Checklist: The authors have completed the STROBE reporting checklist. Available at https://qims.amegroups.com/article/view/10.21037/qims-24-1570/rc

Funding: This work was supported by the National Natural Science Foundation of China (No. 82272078).

Conflicts of Interest: All authors have completed the ICMJE uniform disclosure form (available at https://qims.amegroups.com/article/view/10.21037/qims-24-1570/coif). M.J. is an employee of United Imaging Healthcare, the manufacturer of the CT system used in this study. The other authors have no conflicts of interest to declare.

Ethical Statement: The authors are accountable for all aspects of the work in ensuring that questions related to the accuracy or integrity of any part of the work are appropriately investigated and resolved. This study was conducted in accordance with the Declaration of Helsinki (as revised in 2013) and was approved by the Ethics Committee of Zhongshan Hospital Affiliated to Fudan University (No. B2022-127R). Informed consent was obtained from all individual participants.

References

1. Vatandoust S, Price TJ, Karapetis CS. Colorectal cancer: Metastases to a single organ. World J Gastroenterol 2015;21:11767-76.
2. Pitroda SP, Chmura SJ, Weichselbaum RR. Integration of radiotherapy and immunotherapy for treatment of oligometastases. Lancet Oncol 2019;20:e434-42.
3. Benson AB, Venook AP, Al-Hawary MM, Arain MA, Chen YJ, Ciombor KK, et al. Colon Cancer, Version 2.2021, NCCN Clinical Practice Guidelines in Oncology. J Natl Compr Canc Netw 2021;19:329-59.
4. Argilés G, Tabernero J, Labianca R, Hochhauser D, Salazar R, Iveson T, Laurent-Puig P, Quirke P, Yoshino T, Taieb J, Martinelli E, Arnold D; ESMO Guidelines Committee. Electronic address: clinicalguidelines@esmo. Localised colon cancer: ESMO Clinical Practice Guidelines for diagnosis, treatment and follow-up. Ann Oncol 2020;31:1291-305.
5. Hou P, Liu N, Feng X, Chen Y, Wang H, Wang X, Liu J, Zhan P, Liu X, Shang B, Shen Z, Wang L, Gao J, Lyu P. A paradigm shift in oncology imaging: a prospective cross-sectional study to assess low-dose deep learning image reconstruction versus standard-dose iterative reconstruction for comprehensive lesion detection in dual-energy computed tomography. Quant Imaging Med Surg. 2024;14:6449-6465.
6. Mohammadinejad P, Mileto A, Yu L, Leng S, Guimaraes LS, Missert AD, Jensen CT, Gong H, McCollough CH, Fletcher JG. CT Noise-Reduction Methods for Lower-Dose Scanning: Strengths and Weaknesses of Iterative Reconstruction Algorithms and New Techniques. Radiographics 2021;41:1493-508.
7. Jensen CT, Gupta S, Saleh MM, Liu X, Wong VK, Salem U, Qiao W, Samei E, Wagner-Bartak NA. Reduced-Dose Deep Learning Reconstruction for Abdominal CT of Liver Metastases. Radiology 2022;303:90-8.
8. Belthangady C, Royer LA. Applications, promises, and pitfalls of deep learning for fluorescence image reconstruction. Nat Methods 2019;16:1215-25.
9. Koetzier LR, Mastrodicasa D, Szczykutowicz TP, van der Werf NR, Wang AS, Sandfort V, van der Molen AJ, Fleischmann D, Willemink MJ. Deep Learning Image Reconstruction for CT: Technical Principles and Clinical Prospects. Radiology 2023;306:e221257.
10. Chang W, Lee JM, Lee K, Yoon JH, Yu MH, Han JK, Choi BI. Assessment of a model-based, iterative reconstruction algorithm (MBIR) regarding image quality and dose reduction in liver computed tomography. Invest Radiol 2013;48:598-606.
11. Volders D, Bols A, Haspeslagh M, Coenegrachts K. Model-based iterative reconstruction and adaptive statistical iterative reconstruction techniques in abdominal CT: comparison of image quality in the detection of colorectal liver metastases. Radiology 2013;269:469-74.
12. Euler A, Stieltjes B, Szucs-Farkas Z, Eichenberger R, Reisinger C, Hirschmann A, Zaehringer C, Kircher A, Streif M, Bucher S, Buergler D, D'Errico L, Kopp S, Wilhelm M, Schindera ST. Impact of model-based iterative reconstruction on low-contrast lesion detection and image quality in abdominal CT: a 12-reader-based comparative phantom study with filtered back projection at different tube voltages. Eur Radiol 2017;27:5252-9.
13. Mileto A, Guimaraes LS, McCollough CH, Fletcher JG, Yu L. State of the Art in Abdominal CT: The Limits of Iterative Reconstruction Algorithms. Radiology 2019;293:491-503.
14. Laurent G, Villani N, Hossu G, Rauch A, Noël A, Blum A, Gondim Teixeira PA. Full model-based iterative reconstruction (MBIR) in abdominal CT increases objective image quality, but decreases subjective acceptance. Eur Radiol 2019;29:4016-25.
15. Liao S, Mo Z, Zeng M, Wu J, Gu Y, Li G, et al. Fast and low-dose medical imaging generation empowered by hybrid deep-learning and iterative reconstruction. Cell Rep Med 2023;4:101119.
16. Wang Q, Xu S, Zhang G, Zhang X, Gu J, Yang S, et al. Applying a CT texture analysis model trained with deep-learning reconstruction images to iterative reconstruction images in pulmonary nodule diagnosis. J Appl Clin Med Phys 2022;23:e13759.
17. Li W, You Y, Zhong S, Shuai T, Liao K, Yu J, Zhao J, Li Z, Lu C. Image quality assessment of artificial intelligence iterative reconstruction for low dose aortic CTA: A feasibility study of 70 kVp and reduced contrast medium volume. Eur J Radiol 2022;149:110221.
18. Hu Y, Zheng Z, Yu H, Wang J, Yang X, Shi H. Ultra-low-dose CT reconstructed with the artificial intelligence iterative reconstruction algorithm (AIIR) in (18)F-FDG total-body PET/CT examination: a preliminary study. EJNMMI Phys 2023;10:1.
19. Mainenti PP, Romano F, Pizzuti L, Segreto S, Storto G, Mannelli L, Imbriaco M, Camera L, Maurea S. Non-

invasive diagnostic imaging of colorectal liver metastases. World J Radiol 2015;7:157-69.
20. Fontarensky M, Alfidja A, Perignon R, Schoenig A, Perrier C, Mulliez A, Guy L, Boyer L. Reduced Radiation Dose with Model-based Iterative Reconstruction versus Standard Dose with Adaptive Statistical Iterative Reconstruction in Abdominal CT for Diagnosis of Acute Renal Colic. Radiology 2015;276:156-66.
21. Richard S, Husarik DB, Yadava G, Murphy SN, Samei E. Towards task-based assessment of CT performance: system and object MTF across different reconstruction algorithms. Med Phys 2012;39:4115-22.
22. McCollough CH, Yu L, Kofler JM, Leng S, Zhang Y, Li Z, Carter RE. Degradation of CT Low-Contrast Spatial Resolution Due to the Use of Iterative Reconstruction and Reduced Dose Levels. Radiology 2015;276:499-506.
23. Shehata MA, Saad AM, Kamel S, Stanietzky N, Roman-Colon AM, Morani AC, Elsayes KM, Jensen CT. Deep-learning CT reconstruction in clinical scans of the abdomen: a systematic review and meta-analysis. Abdom Radiol (NY) 2023;48:2724-56.
24. Greffier J, Hamard A, Pereira F, Barrau C, Pasquier H, Beregi JP, Frandon J. Image quality and dose reduction opportunity of deep learning image reconstruction algorithm for CT: a phantom study. Eur Radiol 2020;30:3951-9.
25. Nakamura Y, Narita K, Higaki T, Akagi M, Honda Y, Awai K. Diagnostic value of deep learning reconstruction for radiation dose reduction at abdominal ultra-high-resolution CT. Eur Radiol 2021;31:4700-9.
26. Lyu P, Liu N, Harrawood B, Solomon J, Wang H, Chen Y, Rigiroli F, Ding Y, Schwartz FR, Jiang H, Lowry C, Wang L, Samei E, Gao J, Marin D. Is it possible to use low-dose deep learning reconstruction for the detection of liver metastases on CT routinely? Eur Radiol 2023;33:1629-40.
27. Park S, Yoon JH, Joo I, Yu MH, Kim JH, Park J, Kim SW, Han S, Ahn C, Kim JH, Lee JM. Image quality in liver CT: low-dose deep learning vs standard-dose model-based iterative reconstructions. Eur Radiol 2022;32:2865-74.
28. Jensen CT, Liu X, Tamm EP, Chandler AG, Sun J, Morani AC, Javadi S, Wagner-Bartak NA. Image Quality Assessment of Abdominal CT by Use of New Deep Learning Image Reconstruction: Initial Experience. AJR Am J Roentgenol 2020;215:50-7.

Cite this article as: Qiu QS, Chen XS, Wang WT, Wang JH, Yan C, Ji M, Dong SY, Zeng MS, Rao SX. Image quality, diagnostic performance of reduced-dose abdominal CT with artificial intelligence model-based iterative reconstruction for colorectal liver metastasis: a prospective cohort study. Quant Imaging Med Surg 2025;15(3):2106-2118. doi: 10.21037/qims-24-1570